Progress in PHOTOVOLTAICS

PROGRESS IN PHOTOVOLTAICS: RESEARCH AND APPLICATIONS
Prog. Photovolt: Res. Appl. (2013)
Published online in Wiley Online Library (wileyonlinelibrary.com). DOI: 10.1002/pip.2345

RESEARCH ARTICLE

An improved circuit model for polymer solar cells

Ankita Gaur[1,2] and Pankaj Kumar[1]*

[1] CSIR-National Physical Laboratory, Dr K S Krishnan Marg, New Delhi 110012, India
[2] Indian Institute of Technology Delhi, Hauz Khas, New Delhi 110016, India

ABSTRACT

Authenticity of conventional circuit model, to interpret the characteristics of polymer solar cells (PSCs) is examined. Conventional circuit model is found to be quite limited, and various assumptions used there are not valid for PSCs. By understanding the nature of photovoltaic characteristics, through detailed investigations, we developed an improved circuit model, which explains correctly the behavior of PSCs under different environmental conditions. Investigations are carried out on the solar cells, made of the blend of regioregular poly(3-hexylethiophene) (P3HT) and phenyl [6,6] C_{61} butyric acid methyl ester (PCBM). The model is developed by treating both the dark and illuminated characteristics separately, even the characteristics were dealt with separately in reverse and forward biases. The formulated equivalent circuit model helps us in explaining many other important features, observed in the characteristics of PSCs. Copyright © 2013 John Wiley & Sons, Ltd.

KEYWORDS
polymer solar cells; equivalent circuit; thin film; P3HT; PCBM

***Correspondence**
Pankaj Kumar, CSIR-National Physical Laboratory, Dr K S Krishnan Marg, New Delhi 110012, India.
E-mail: pankaj@mail.nplindia.ernet.in

Received 28 April 2012; Revised 7 September 2012; Accepted 13 November 2012

1. INTRODUCTION

Polymer solar cells (PSCs) have evolved as truly promising and cost effective alternates to traditional solar cells [1–3]. Ease in roll-to-roll fabrication, thin and lightweight make this technology more attractive. In the last decade, research has accelerated and the number of research publications on PSCs has increased exponentially. Intermixing of donor–acceptor materials into a single layer (bulk heterojunction; BHJ) has revolutionized the technology. Understanding the device physics, devices engineering and application of advanced materials have resulted into rather efficient devices [4–8]. One decade before, efficiency hardly reached beyond 2% but now efficiencies exceeding 8% have been reported in BHJ structures [9–12]. Although there have been great improvements in efficiency via improvements in short circuit current density (J_{sc}), open circuit voltage (V_{oc}) and fill factor (FF) through materials and device engineering [4,8], there is still enough space to improve them further. Apart from high efficiency, long-term durability is another important issue, which is technologically equally important. Development in just only one area would not serve the purpose and will keep the technology away from the society. Focused research is oriented in this direction too and few PSCs have shown outdoor working lifetime of ~10 000 h [13–15], but it is worth mentioning that this durability is not for the devices exhibiting high efficiency, therefore PSCs with high efficiency and high durability are still to be realized. Overall the present performance of PSCs is not high enough to seek commercial place and more developments are essentially required. Recent research trends show the main focus on development of solar cells with high performance in terms of high efficiency and long durability [16–18]. Stable solar cells can be realized with high thermal, electrochemical and oxidizing stability of organic molecules. It is anticipated that PSCs having efficiency of ~10% with lifetime of >50 000 h will become a strong competitor to conventional c-Si solar cells and can be expected in the market [2].

Device modeling and understanding the physics behind operation, help us in mapping the parameters that affect the performance of a solar cell. Modeling is an important tool and a correct model will help us in achieving highly efficient and stable solar cells. Our aim is to develop an equivalent circuit model for PSCs that helps in explaining the nature of characteristics and understanding their qualitative and quantitative losses. Although the basic principle is same but PSCs differ in many ways from c-Si solar cells, viz. structural design, active layer possesses

two different materials called electron donor and acceptor, incident photons generate bound electron–hole pairs called excitons (binding energy ~0.5 eV), charge carrier mobilities are low and the materials possess fast degradation. Excitons are the neutral quasi-particles with finite lifetime and finite diffusion length. PSCs possess two electrodes with the active organic materials sandwiched between them, where at least one of the electrodes is optically transparent. Thermal energy at room temperature is not sufficient enough to break the excitons into free charge carriers; therefore after light absorption, the photo-generated excitons have to diffuse to the donor–acceptor interface to dissociate into electrons and holes via an ultra-fast charge transfer process. Excitons not reaching the interface decay radiatively or non-radiatively. As exciton diffusion lengths are considerably smaller than the required thickness of the active layer for efficient light absorption, therefore some of the excitons do no contribute to photo-current and recombine. The dilemma was overcome by intermixing of donor–acceptor materials that form donor–acceptor interfaces throughout entire bulk of the active layer and within the diffusion lengths of excitons. Now excitons dissociate efficiently (~100%) [19], into electrons and holes before they recombine. Even after dissociation, due to coulombic attraction, some geminate pairs of electrons and holes are formed across the interface, which are called charge transfer states (CTSs) and needs to be dissociated into free electrons and holes [20]. The necessary force to dissociate CTSs into free charge carriers is provided by internal electric field and the probability of dissociation is described by the Onsager–Braun model [21]. The separated electrons and holes transport through the respective channels (electrons in acceptor channel and holes in donor channel) to collect at the respective electrodes. The separated charge carriers may recombine at the interface or may become trapped into localized states while transporting, which results into reduced photocurrent. The surviving charge carriers are extracted out of the cell via drift–diffusion process and formulate a photocurrent. Charge transport usually happens via hopping phenomenon from one localized state to another. As a whole, the extracted photocurrent does not solely depend on photo-generation of excitons but also on the exciton diffusion, excitons dissociation and charge transport properties of the donor/acceptor materials. The photovoltaic response of a cell changes with variation in the active layer morphology, which depends on the compatibility of intermixing of donor–acceptor materials, their ratio, solvent used, growth rate of active layer and post-production treatments [6,9,22–24].

To a reasonable limit, the conventional circuit model used for inorganic solar cells (one-diode model), has been used to interpret the behavior of PSCs as well [25,26]. However, as the dark and photovoltaic response of PSCs happen to be quite different from those of inorganic counterparts, different equivalent circuit models were developed and used to explain the characteristics of PSCs [25,27–29]. Single diode model [25,30], two-diode model [27] and three-diode model [28] are the most important models and are shown in Figure 1. The light contribution in these models is represented by a constant current source whereas the rest of the circuits correspond to dark

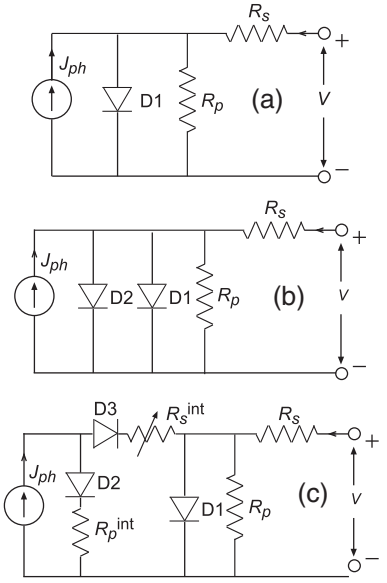

Figure 1. (a) One-diode model [29], (b) two-diode model [27] and (c) three-diode model for solar cells [28].

component. Single diode and two-diode models are extensively used for inorganic solar cells [29]. The two-diode model consists of an additional diode connected in parallel to the original diode in the same polarity. For the second diode, the reverse saturation current density corresponds to the deep-level recombination in space charge region and is generally three to seven orders of magnitude larger than that for original diode. Mazhari presented an improved three-diode model for PSCs under illumination [28]. The work of Mazhari is quite appreciable as it explains the characteristics of PSCs under illumination, but it is quite limited and does not explain some other important features of PSCs. We have analyzed the validity of these circuit models and found various discrepancies. We have performed detailed investigations on solar cells based on the blend of poly(3-hexylethiophene) (P3HT) and phenyl [6,6] C_{61} butyric acid methyl ester (PCBM) and developed a model for *J–V* characteristics, which helped us in developing the equivalent circuit model. The improved circuit model helped us in interpreting many important features of PSCs.

2. THE CONVENTIONAL ONE DIODE CIRCUIT MODEL

Before understanding the behavior of PSCs, let us have a look on the characteristics and circuit model of conventional inorganic solar cells. For a conventional Si *p–n* junction solar cell, the *J–V* relation in dark is given by [29]

$$J = J_s\left(\exp\left(\frac{q(V - JAR_s)}{nkT}\right) - 1\right) + \frac{V - JAR_s}{AR_p}, \quad (1)$$

where J_s is reverse saturation current density, n is ideality factor, R_s and R_p are respectively the parasitic series and shunt resistances, A is active area of the cell, k is Boltzmann constant and T is the absolute temperature. Under illumination J–V relation modifies to [29]

$$J = J_s\left(\exp\left(\frac{q(V - JAR_s)}{nkT}\right) - 1\right) + \frac{V - JAR_s}{AR_p} - J_{ph}, \tag{2}$$

where J_{ph} is photo-generated current density in the cell. It is assumed here that for a given illumination intensity, the photocurrent remains constant in magnitude and is independent of applied voltage. This equation is based on the superposition principle of current densities, and in forward bias, the direction of flow of photo-generated current is opposite to that of dark current. For a given set of parameters, Figure 2 shows the plots of Equation (2) in dark and under illumination. The corresponding equivalent circuit is shown in Figure 1(a). The forward bias characteristic in dark can be divided into three regions mainly *A-B*, *B-C* and *C-D*. Region *A-B* shows ohmic conduction and is due to leakage current through R_p until the current through diode D1 is sufficiently large. Region *B-C* shows exponential variation of current with voltage and is controlled by the diode D1 whereas in region *C-D*, current becomes very large and potential drop across R_s becomes important and therefore the current is controlled by R_s along with diode D1. In reverse bias, the characteristic shows ohmic nature in the entire voltage range *A-E* and is due to leakage current through R_p only, as it is more than the reverse saturation current density through D1. Under illumination the voltage corresponding to zero output current is called V_{oc} whereas current density at zero applied voltage is called J_{sc}, which is supposed to be equal to photocurrent generated in the cell (J_{ph}), however it is not true as some part

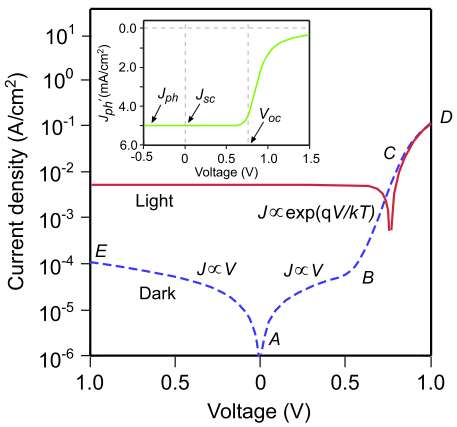

Figure 2. Calculated dark and illuminated J–V characteristics of a Si-solar cell with $J_s = 3.38 \times 10^{-11}$ A/cm^2, $n = 1.6$, $R_s = 10\,\Omega$, $R_p = 1 \times 10^5\,\Omega$, $A = 0.1$ cm^2, $J_{ph} = 5$ mA/cm^2 and $T = 295$ K. Inset shows the photocurrent contribution (J_{ph}') obtained by subtracting the output of Equation (2) from that of Equation (1).

of photocurrent would recombine through R_p. If R_p is large and R_s is very low, J_{sc} may be approximately equal to J_{ph}. In that case, V_{oc} of the cell can be found from

$$J_s\left(\exp\left(\frac{qV_{oc}}{nkT}\right) - 1\right) + \frac{V_{oc}}{AR_p} - J_{ph} = 0. \tag{3}$$

Calculations show that for low values of R_p, V_{oc} becomes small as the large part of photocurrent would pass through R_p and photocurrent contribution through R_s would decrease. Therefore to make the total current zero at output (condition for V_{oc}), small applied voltage will be required. For smaller values of R_p, V_{oc} increases with R_p, however for large values of R_p, V_{oc} becomes saturated. R_s is found to have no effect on V_{oc} but it affects the photocurrent extracted out of the cell. Based on the superposition principle, the photocurrent contribution extracted out of the cell (J_{ph}') through R_s can be obtained by subtracting the dark current from the current under illumination. Inset of Figure 2 shows the variation of J_{ph}' as a function of applied voltage, obtained from the difference of two currents from Equations (1) and (2). It is seen that J_{ph}' remains equal to J_{ph} in reverse bias, whereas in forward bias it remains almost equal to J_{ph} for low voltages and decreases as the applied voltage increases. It is because when in reverse bias D1 is *off* and current through R_p is small, J_{ph}' may be equal to J_{ph}, but when in forward bias D1 is *on*, a large part of photocurrent would recombine through D1 and R_p, which will result into reduction in J_{ph}'. Or in other words, under illumination some additional current would flow through R_p and D1, which will increase voltage drop across R_p, therefore at a given applied voltage, voltage drop and current through R_s would decrease. At V_{oc}, J_{ph}' is equal and opposite to dark current through R_s due to applied voltage, which results into a net zero current through R_s. When the applied voltage increases beyond V_{oc}, J_{ph}' decreases first rapidly and then very slowly with voltage, and at very large voltages it becomes negligible. It is worth mentioning here that for $V > 0$, the photocurrent generated in the cell (J_{ph}) does not actually change but it remains constant and only its contribution at the output terminals (J_{ph}') changes with the applied voltage due to some recombination through D1 and R_p.

3. EXPERIMENTAL PROCEDURE

P3HT and PCBM is one of the best and most studied donor–acceptor combination for PSCs, which have shown high performance both in terms of efficiency and environmental stability. Therefore to formulate equivalent circuit model for PSCs, we carried out the investigations on solar cells based on this system. Pre-patterned indium tin oxide (ITO) coated glass substrates were first cleaned mechanically in detergent and distilled water and then subsequently cleaned with acetone, trichloroethylene and isopropanol. Substrates were dried in vacuum oven and then exposed to air plasma for 5 min. Poly(ethylenedioxythiophene) : poly styrene sulfonate (PEDOT : PSS)

was spun on the ITO substrates at 2000 rpm for 2 min and cured at 120 °C for 10 min in vacuum oven. After that 1 : 0.5 wt% blend of P3HT (Aldrich Chemicals, USA) and PCBM (Nano-C, USA) prepared in chlorobenzene (25 mg/ml) was spun on a PEDOT : PSS layer in a glove box. The samples were then cured at 120 °C for 30 min. resulting into ~104 nm of P3HT : PCBM active layer, as measured with an ellipsometer of J. A. Woollam, USA. The substrates were then transferred into a vacuum evaporation chamber where Al electrodes were evaporated at a base pressure of $\sim 1 \times 10^{-6}$ Torr, on the active layer through shadow masks, defining a cell area of ~0.04 cm^2. After preparation, the samples were taken out of the evaporation chamber and *J–V* characteristics were measured in dark and under illumination in ambient conditions (43% rh, 27 °C) using Keithley 2420 SourceMeter unit, interfaced with computer. Measurements were performed in forward sweep of the applied voltage viz. from −1 to +1 V in the steps of 200 mV. W-halogen lamp from OSRAM, Germany was used to illuminate the cells at different illumination intensities.

4. MODELING OF IMPROVED CIRCUIT MODEL FOR PSCS

4.1. Analysis of dark *J–V* characteristics

For detailed understanding, we performed the experiments at different illumination intensities and the measured *J–V* characteristics are shown by symbols in Figure 3. Nature of the characteristics seems to be quite similar to those shown in Figure 2, but detailed analysis shows that they cannot be explained by Equation (2), as the electronic properties of organic materials and cell structures are entirely different from those of inorganic solar cells. Charge transport in organic materials is expected to be

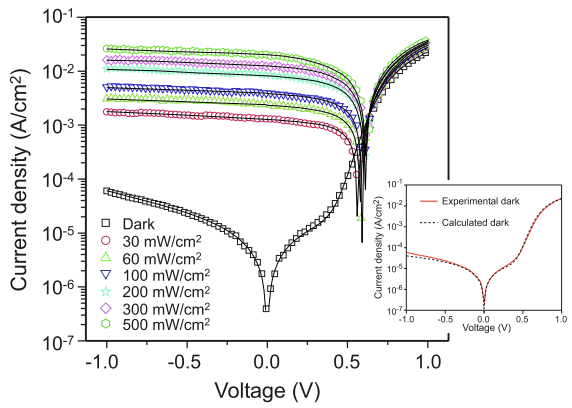

Figure 3. Dark and illuminated *J–V* characteristics (symbols) of ITO/PEDOT : PSS/P3HT : PCBM/Al solar cell measured at room temperature in ambient environment. Dark solid curves are the plot of Equation (10) at different illumination conditions where $J_{ph}(V)$ is given by Equation (11). Inset shows the comparison of Equation (8) (calculated dark) with experimental dark characteristics.

space charge limited [31]; however at low voltages, the effect of built-in voltage (V_{bi}) due to asymmetric electrodes and diffusion of charge carriers cannot be ignored. As electrons transport in acceptor channel and holes in donor channel, *J–V* characteristics of PSCs can be modeled by considering the active layer to be single virtual semiconductor with highest occupied molecular orbital (HOMO) level equal to that of donor and lowest unoccupied molecular orbital (LUMO) level equal to that of acceptor [32]. In that case electron and hole mobilities of the virtual semiconductor are respectively considered to be equal to the electron mobility of acceptor and hole mobility of donor. In that case, physics of PSCs will be based on the physics of metal–insulator–metal (MIM) diode. Calculations show that if the contacts are not ohmic in MIM diode, the internal electric field remains constant for low applied voltages; however at large applied voltages, effect of diffusion may become negligible and the field distribution will not be constant. Impedance spectroscopy is an important tool to characterize PSCs [33]. For ohmic contacts, the field will not be constant in the vicinity of the contacts; however, it will be constantly far away from the contacts [32,34]. Now assuming non-ohmic contacts, the solution of current density and Poisson's equations for electrons, in steady-state and low voltage region gives [32]

$$J_n = \frac{q^2 D_n N_c (V_{bi} - V) \exp\left(\frac{-\phi_1}{kT}\right)\left(\exp\left(\frac{qV}{kT}\right) - 1\right)}{dkT\left(1 - \exp\left(\frac{-q(V_{bi}-V)}{kT}\right)\right)}, \quad (4)$$

where N_c is the effective density of states for conduction band, ϕ_1 is the injection barrier for electrons from anode, $D_n = \frac{\mu_n kT}{q}$, μ_n is the electron mobility, d is the sample thickness and $qV_{bi} = \phi_1 - \phi_2$ where ϕ_2 is the electron injection barrier from cathode. V_{bi} is the built-in property of a cell and depends on the electrode materials. In a semiconductor if recombination/generation is considered, it can be either be band to band or trap assisted recombination. Because we have considered electron and hole transport through different channels (electrons in acceptor channel and holes in donor channel), the probability of band-to-band recombination/generation is reduced and trap-assisted recombination/generation becomes more probable. The current due to trap-assisted recombination can be given by integration of trap-assisted Shockley–Read–Hall recombination rate [29] and now Equation (4) would modify to

$$J_n = J_{n0}(V)\left(\exp\left(\frac{qV}{nkT}\right) - 1\right), \quad (5)$$

where $J_{n0}(V) = \frac{q^2 D_n N_c (V_{bi}-V)\exp\left(\frac{-\varphi_1}{nkT}\right)}{dnkT\left(1-\exp\left(\frac{-q(V_{bi}-V)}{nkT}\right)\right)}$ and n is the ideality factor. Hole current density can also be given by a similar expression and the total current through the diode would be given by

DOI: 10.1002/pip

$$J = \left(J_{n0}(V) + J_{p0}(V)\right)\left(\exp\left(\frac{qV}{nkT}\right) - 1\right), \quad (6)$$

or

$$J = J_s(V)\left(\exp\left(\frac{qV}{nkT}\right) - 1\right). \quad (7)$$

where $J_s(V) = J_{n0}(V) + J_{p0}(V)$. For a practical case where parasitic R_s and R_p become important, the current through the cell would be given by

$$J = J_s(V - JAR_s)\left(\exp\left(\frac{q(V - JAR_s)}{nkT}\right) - 1\right) + \frac{V - JAR_s}{AR_p}. \quad (8)$$

R_s and R_p in PSCs come from the resistivity of organic materials, contact metal electrodes and metal-organic interfaces. Equation (8) is similar to Equation (1), except the reverse bias current density is not constant but some function of applied voltage. Equation (8) explains well the nature of dark characteristics of PSCs in forward bias, as Equation (1) does for Si solar cells. However at very high voltages, the effect of diffusion will become negligible and the charge carrier transport would be controlled by space charge limited conduction [35] and Equation (8) will no longer be valid. Even for the best fitting of Equation (8) with experimental data in forward bias, the plot of Equation (8) did not follow experimental data in reverse bias (see inset of Figure 3). The values of different parameters are the same as those for lowest solid curve in Figure 3 (given subsequently), with $J_{s2} = 0$. However Equation (8) showed a reasonable fit in reverse bias for low voltages only. Low voltage region in reverse bias corresponds to ohmic conduction, which is in good agreement with Equation (8), but at higher voltages current varies exponentially with applied voltage (Shockley kind). The cells prepared in different processing conditions revealed that the nature of characteristics depends on the quality of the cell. In some cases, this exponential variation may not happen even for very large voltages, and in other cases, the variation may not be exponential but space charge limited. This different nature of characteristics in reverse bias, forced us to rethink on this issue and to develop a suitable model. Such a nature of characteristics could be explained by introduction of another diode D2 in equivalent circuit, connected in parallel but in opposite polarity to the existing diode D1 of conventional circuit model (see Figure 4(a)). Due to non-linear nature of characteristics in reverse bias, the use of a diode is justified.

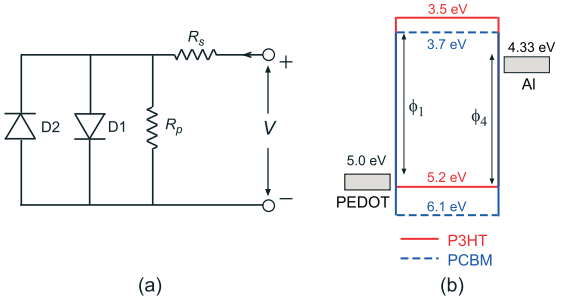

Figure 4. (a) Improved equivalent circuit for PSCs in dark and (b) schematic representation of energy levels of different materials in ITO/PEDOT : PSS/P3HT : PCBM/Al solar cell.

Depending on the cell structure and its properties, the current through diode D2 may be exponential in voltage or space charge limited. Diode D2 will have different values of parameters than those for D1. For low reverse bias, the leakage current through R_p would be more than the current through D2; however, for high reverse bias the current through D2 would dominate. It is worth mentioning that even with pure ohmic conduction in reverse bias the characteristics can even be modeled by introduction of D2, although the current through it would be negligible in that case. As in present case, characteristics in reverse bias show exponential variation with voltage, Equation (8) can be modify to

$$J = J_{s1}(V - JAR_s)\left(\exp\left(\frac{q(V - JAR_s)}{n_1 kT}\right) - 1\right) - J_{s2}\left(\exp\left(\frac{-q(V - JAR_s)}{n_2 kT}\right) - 1\right) + \frac{V - JAR_s}{AR_p} \quad (9)$$

where $J_{s1}(V - JAR_s)$ and J_{s2} are respectively the reverse bias current densities in D1 and D2, n_1 and n_2 are the ideality factors of the respective diodes. The lowest dark solid curve in Figure 3 is the plot of Equation (9), which shows an excellent agreement with dark J–V characteristic in both the forward and reverse biases. The corresponding values of parameters are $N_c = N_v = 10^{19}/\text{cm}^3$, $d = 104$ nm, $\mu = 2.6 \times 10^{-4}\,\text{cm}^2/\text{V s}$, $\phi_1 = 1.3$ eV, $\phi_4 = 0.87$ eV, $V_{bi} = 0.66$ eV, $n_1 = 1.35$, $R_s = 1\ \Omega$, $R_p = 1.23 \times 10^6\,\Omega$, $A = 0.04\,\text{cm}^2$, $T = 295$ K, $J_{s2} = 4 \times 10^{-7}\,\text{A/cm}^2$ and $n_2 = 12$. ϕ_4 is the hole injection barrier from cathode. The values of ϕ_1, ϕ_4 and V_{bi} are calculated from the energy levels of different materials shown in Figure 4(b). The values of energy levels of different materials and μ are taken from the literature and are approximately equal to the experimentally determined values. The value of V_{bi} is in quite agreement as measured from the intersection of dark and illuminated J–V characteristics [36]. Values of R_s, R_p, J_{s2} and n_2 are obtained by the fitting of the J–V characteristics. Please note that for different nature of characteristics in reverse bias, the second term in Equation (9) (corresponding to D2) would have to modify accordingly and the values of parameters will be different.

4.2. Analysis of illuminated *J–V* characteristics

To model the illuminated characteristics, it is utmost important to calculate first the photo-generated current in the PSCs. Photocurrent in a PSC can be obtained by calculating the external quantum efficiency (EQE), where the optical losses, actual absorption profile, charge carrier generation and losses during charge carrier transportation play important role [2,37,38]. Once the EQE is known, photocurrent generated in the cell can be calculated by integrating EQE over the absorption spectral range. A central assumption in conventional model is that photo-generated current density (J_{ph}) is constant for a given illumination intensity and independent of applied voltage, but this assumption does not hold for PSCs. Photocurrent in PSCs is constant for constant illumination intensity but it varies with applied voltage. In order to examine the validity of this assertion, we did calculate the photocurrent contributions at output terminals (J_{ph}') through R_s, for different illumination intensities and are shown in Figure 5 as a function of applied voltage. J_{ph}' has been calculated by subtracting the dark current from the current under illumination. It is found that for all the illumination intensities, J_{ph}' remains negative in the direction for $V<0$ and varies slight linearly, whereas for $V>0$, it decreases first slowly and then rapidly with applied voltage. For all illumination intensities, J_{ph}' becomes zero at 0.66 V and for $V>0.66$ V, it becomes positive in the direction and increases with applied voltage. These results are quite contrary to those observed in Figure 2. Also according to the model proposed by Mazhari, J_{ph}' can be zero but the direction will not change [28]. Therefore because of vanishing character for $0<V<0.66$ V and change in direction for $V>0.66$ V, J_{ph} cannot be considered constant with applied voltage, as assumed by many authors [25,26,39]. These results suggest J_{ph} to be a function of applied voltage. Therefore under illumination, the *J–V* relation for PSCs should be written as

$$J = J_{s1}(V - JAR_s)\left(\exp\left(\frac{q(V - JAR_s)}{n_1 kT}\right) - 1\right) - J_{s2}\left(\exp\left(\frac{-q(V - JAR_s)}{n_2 kT}\right) - 1\right) + \frac{V - JAR_s}{AR_p} - J_{ph}(V), \qquad (10)$$

where $J_{ph}(V)$ is the photocurrent generated in the cell. The function which defines the relation between J_{ph} and V is important to understand. We established the relation between J_{ph} and V by critically analyzing the *J–V* characteristics under illumination.

It is worth mentioning again that in BHJ solar cells the exciton dissociation efficiency is ~100%, but after exciton dissociation, the charge collection efficiency depends on drift length of the charge carriers, which is given by $\mu\tau E_{eff}$, where μ is the carrier mobility, τ is the carrier lifetime and E_{eff} is the effective electric field in the cell, which can be written as $(V_{bi}-V)/d$. Despite diffusion, the internal electric field provides necessary force (drift) to collect the charge carriers at respective electrodes. Charge carriers do not recombine within the drift length, but beyond the drift length, charge carriers do not survive and recombine through traps. If drift length of charge carriers is more than the thickness of active layer, then only all photo-generated charge carriers are expected to be collected, otherwise only the charge carriers within drift length will be collected and the rest will recombine. As the applied voltage increases in forward bias, E_{eff} decreases, and for $V=V_{bi}$, E_{eff} will vanish and there will be no extraction of photo-generated charge carriers (if diffusion is ignored) and all of them will recombine. This is exactly the situation seen in Figure 5, where photocurrent becomes 0 at 0.66 V. For $V>0.66$ V, the direction of photocurrent is reversed and is consistent with the situation that for $V>V_{bi}$, the direction of E_{eff} will be reversed, and it reverses the direction of $J_{ph}(V)$. These observations suggest J_{ph} to be a function of E_{eff}. On the basis of the drift length concept Brabec *et al.* proposed $J_{ph}(V)$ to be a linear function of E_{eff} given by $J_{ph}'' \frac{\mu\tau E_{eff}}{d^2}$, where J_{ph}'' is the maximum possible photocurrent generated in the cell and is constant for a given illumination intensity and independent of applied voltage [30]. If $\mu\tau E_{eff}>d$, J_{ph} will be equal to J_{ph}'', although the direction will depend on the direction of E_{eff}, which will also depend on the magnitude of applied voltage V.

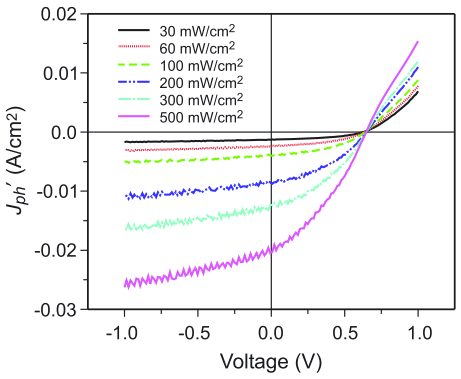

Figure 5. Variation of extracted photocurrent contribution (J_{ph}') with applied voltage at different illumination intensities.

For $V<0$, photocurrent would flow in the same direction as that of dark current. Although for $0<V<V_{bi}$, magnitude of photocurrent would decrease but direction will still be the same but opposite to that of the dark current. But for $V>V_{bi}$ the direction of photocurrent would change and the magnitude will increase with applied voltage until it saturates. Now both the dark current and photocurrent are in the same direction. It is important to note that usually photocurrent becomes zero at $V=V_{bi}$, but it is not a necessary condition for all organic solar cells. For example at $V=V_{bi}$, the drift component of photocurrent becomes 0 but even then we may obtain photocurrent because of diffusion of the charge carriers. This is an important case for bilayer solar cells [40]. In that case V_{oc} will be more than V_{bi} and the intersection voltage of dark and illuminated characteristics, where

photocurrent becomes 0, will be more than V_{bi}. If diffusion is not important, the photocurrent would be determined by drift and then intersection point will be equal to V_{bi} and in that case V_{oc} will be less than V_{bi}. In BHJ solar cells, diffusion becomes negligible if intensity distribution is uniform. As we are modeling the characteristics for BHJ solar cells, where charges are generated throughout the cell, we can ignore the effect of diffusion, and photocurrent becoming 0 at $V = V_{bi}$ would be a good approximation.

According to the aforementioned model $J_{ph}(V)$ is expected to be equal to J_{ph}'' for high internal electric fields. Calculations show that even at $V = 0$ V, the internal electric filed in the present sample due to V_{bi} is sufficiently enough for $\mu\tau E_{eff} > d$ and the photocurrent is expected to be saturated at 0 V, but rather illuminated current varies slight linearly in reverse bias. This is because of some polaron pair recombination at donor–acceptor interface due to Coulombic attraction between electrons and holes. Now application of reverse bias is expected to provide sufficient force for collection of all the photo-generated charge carries and to obtain saturation in photocurrent. This statement became clearer with the measurements performed at relatively higher voltage range. Figure 6 shows the dark and illuminated J–V characteristics of the cell measured in the voltage range of ± 3.5 V. Variation in J_{ph}' with applied voltage in this case is shown in the inset of the figure. In reverse bias, initially for up to~-1.2 V, J_{ph}' varies slight linearly with applied voltage and then interestingly it saturates at ~-1.5 V. Two solid lines have been plotted in the inset just to show the linear variation and saturation in J_{ph}'. But more interestingly, for higher voltages beyond -2.7 V, J_{ph}' started decreasing. Please do not confuse that this reduction is because of reduction in $J_{ph}(V)$ after saturation, but it is because $J_{ph}(V)$ is saturated at J_{ph}'' but dark current is still increasing with applied voltage; therefore, the difference of two currents (J_{ph}') tends to 0. In forward bias J_{ph}' varies nonlinearly in the fourth quadrant, where it decreases first slowly and then rapidly with applied voltage and becomes zero at 0.66 V. As the voltage increases further, J_{ph}' becomes reversed in direction and starts increasing rapidly. These results are consistent with those observed for lower voltage range (Figure 5). But interestingly after ~1.7 V, J_{ph}' starts decreasing and can be attributed to the same effect observed in reverse bias beyond -2.7 V, where photocurrent is saturated and dark current increases with applied voltage, resulting J_{ph}' tending to 0.

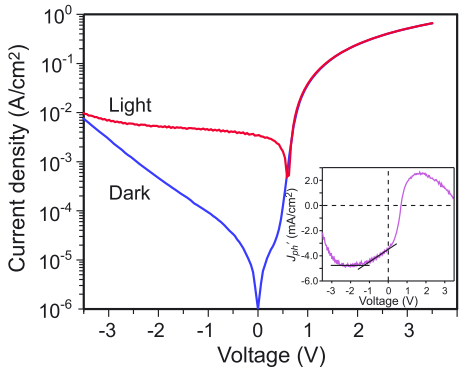

Figure 6. Dark and illuminated (100 mW/cm^2) J–V characteristics of ITO/PEDOT : PSS/P3HT : PCBM/Al solar cell measured at higher voltage range. Inset shows the variation of extracted photocurrent contribution (J_{ph}') with applied voltage. Solid lines in inset have just been plotted to guide the eyes about the trend in variation.

We tried to fit the illuminated characteristics with Equation (10), using the same values of parameters as those in dark and considered $J_{ph}(V)$ to be a linear function of E_{eff}. The characteristics did not show agreement in forward bias ($V > 0$) but a reasonably good fit was observed in reverse bias ($V < 0$). However, a rough fitting was observed for $0 < V < V_{bi}$ with slight reduction in shunt resistance. As for $0 < V < V_{bi}$, J_{ph}' varies nonlinearly with applied voltage, the assumption that $J_{ph}(V)$ varies linearly with E_{eff} gave a rough fitting, which is not acceptable. An excellent fitting was observed for $V < 0$ and $V < V_{bi}$ by considering $J_{ph}(V)$ to be an exponential function of $(V_{bi} - V)$, of the form $J_{ph}''\left(1 - \exp\left(\frac{V - V_{bi} - J_{ph}(V)AR_{s2}}{n_3 kT}\right)\right)$, where n_3 is the ideality factor and R_{s2} is the effective series resistance under illumination. The fitting was excellent for all illumination intensities and with the same values of diode parameter as those in dark except reduction in shunt resistance and increment in series resistance with illumination intensity. As illumination intensity increases, shunt resistance reduces further and series resistance increases. Reduction in shunt resistance under illumination is quite acceptable and has been observed by many authors [30,32]. Reduction in shunt resistance can be attributed to the photo-induced doping and can be represented by adding a parallel resistance R_{p2} where photoconductivity is proportional to incident illumination intensity. In order to estimate the contribution of this effect to the existing shunt resistance, the photoconductivity will have to be weighted by the probability of the charge carriers of one type to penetrate the barrier presented by the selective electrodes. Waldauf *et al.* called this weighing factor as the contact permeability (CP) [41]. The CP can be estimated by curve fitting of J–V characteristics of illuminated solar cell under reverse bias. On the other hand, increment in series resistance can be attributed to difficulty in extraction of charge carriers due to space charge effect, which increases with illumination intensity and can be represented by addition of a series resistance R_{s2} to photocurrent extraction. For $V > V_{bi}$, the characteristics did show agreement with none of the aforementioned functions. Because for $V > V_{bi}$ the direction of photocurrent is changed, the collection of photo-generated charge carriers will be at opposite electrodes. Although in principle there should not be any change in photovoltaic behavior but as the interfaces for charge extraction are changed, the photo-physical properties of the cell will change and even the magnitude of extracted photocurrent may change. The exact reason behind is not very much clear at this stage and it requires more detailed investigations further; therefore, we are leaving this issue for future endeavors. However for $V > V_{bi}$, the excellent

agreement could be achieved with the experimental data by considering $J_{ph}(V)$ to be an exponential function of the form $-J_{ph}''\left(1-\exp\left(\frac{V-V_{bi}-J_{ph}(V)AR_{s2}}{n_4kT}\right)\right)$, until it saturates to some multiple of J_{ph}''. Here n_4 is the ideality factor. It is the same function as used for $V<V_{bi}$ except the ideality factor is different. With these assumptions, we were able to have an excellent fit for $V>V_{bi}$ for all illuminated intensities. As a whole, $J_{ph}(V)$ could be written as

$$J_{ph}(V)=J_{ph}'' \text{ for} V<0,$$
$$J_{ph}(V)=J_{ph}''\left(1-\exp\left(\frac{V-V_{bi}-J_{ph}(V)AR_{s2}}{n_3kT}\right)\right) \text{ for } 0<V<V_{bi}$$

and

$$J_{ph}(V)=-J_{ph}''\left(1-\exp\left(\frac{V-V_{bi}-J_{ph}(V)AR_{s2}}{n_4kT}\right)\right) \text{ for } V>V_{bi} \quad (11)$$

Dark solid curves in Figure 3 are the plots of Equation (10) where $J_{ph}(V)$ is given by Equation (11). The modeled characteristics show excellent agreement with experimental data at different illumination intensities. The values of R_s and R_p for different illumination intensities are given in Table I. Values of the rest of the parameters are the same as those in dark with $n_3=6.7$ and $n_4=8.0$. While calculating the photocurrent, we considered equal contribution from both the photo-generated electrons and holes.

On the basis of the experimental observations and model presented earlier, we extended the dark equivalent circuit model (Figure 4(a)) to that under illumination and is shown in Figure 7. As discussed earlier the extracted photocurrent does not solely depend on the photo-generation of excitons but also on the exciton diffusion, excitons dissociation and charge transport properties of the donor–acceptor materials; therefore, it will depend on the competition between recombination and extraction of charge carriers. Under illumination, we may consider addition of a current source to the dark circuit with recombination and collection provisions. Because photo-physical properties of studied cell are different for $V<V_{bi}$ and $V>V_{bi}$, the circuit can be modeled by considering two independent light sources, one of which contributes for $V<V_{bi}$ and other for $V>V_{bi}$. The two sources are

Table I. Variation in fitted values of R_s and R_p with illumination intensity.

Illumination intensity (mW/cm^2)	R_s (Ω)	R_p (Ω)
30	1	1.0×10^5
60	10	7.8×10^4
100	60	4.9×10^4
200	120	2.5×10^4
300	160	2.2×10^4
500	180	1.6×10^4

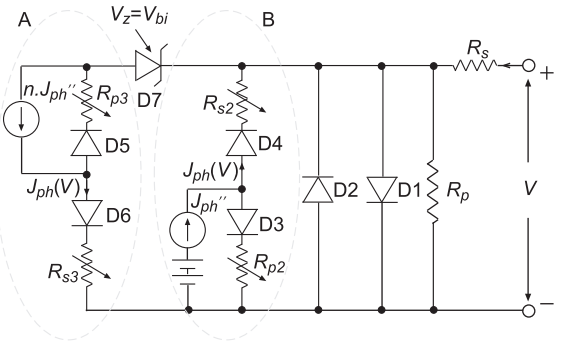

Figure 7. Improved equivalent circuit model for PSCs under illumination.

connected in such a way that one is active for $V<V_{bi}$ and other for $V>V_{bi}$. In that case, the two sources may be considered connected through an ideal zener diode with zener voltage equal to V_{bi}, which is connected in reverse bias such that it is short circuited for $V>V_{bi}$ and open circuited for $0<V<V_{bi}$. As discussed earlier, recombination and collection happen in both the cases; therefore, such behavior can be described by introduction of two additional diodes along with series and shunt resistances such that one diode is for recombination losses and the other is for charge collection [28].

To understand in detail, let us discuss the two cases separately, where the first case is $V<V_{bi}$. As discussed earlier the illumination part cannot be represented by a constant current source, but it should be a source whose output changes with applied voltage until it reaches its maximum value, which is constant for a given illumination intensity. The maximum photocurrent corresponds to the net generation rate of excitons in the cell. Therefore, the current source (encircled portion B, Figure 7), comprises a voltage source with potential nearly equal to V_{bi} and a reservoir of charge carriers that can provide the charge carriers to flow, giving a maximum current of J_{ph}''. For low internal electric fields, all the charge carriers will not be extracted out and recombination will happen at the dissociating interface and in bulk of the active layer. Therefore, recombination and extraction of charge carriers are accounted through photo-induced R_{p2} and R_{s2} along with diodes D3 and D4, in such a way that it represents characteristics of PSCs. Use of photo-induced R_{p2} and R_{s2} is essential to justify the reduction in shunt resistance under illumination. The value of R_{p2} changes with illumination intensity. Exponential variation of photocurrent can be justified by the use of diodes. The diodes D3 and D4 are connected in such a way that they become important under illumination only. In dark, these diodes are reverse biased and have no impact on *J–V* characteristics of the cell. The current through D3 along with shunt resistance R_{p2} corresponds to recombination current, whereas current through D4 along with series resistance R_{s2} corresponds to $J_{ph}(V)$. In short circuit condition, both the D3 and D4 will be *on*, and we have

$$J_{sc} = J_{ph}(0) - J_{RP} - J_{D1} \quad (12)$$

where $J_{ph}(0) = J_{ph}'' - \frac{V_{bi}}{AR_{p2}}$, because some part of photocurrent would recombine through R_{p2}, J_{RP} and J_{D1} are the currents through R_p and D1 therefore,

$$J_{sc} = J_{ph}'' - \frac{V_{bi}}{AR_{p2}} - \frac{J_{sc}R_s}{R_p} - J_s\left(\exp\left(\frac{qJ_{sc}AR_s}{nkT}\right) - 1\right) \quad (13)$$

Equation (13) inferences clearly that J_{sc} depends critically on R_{p2} and R_s. If R_{p2} is small, the internal recombination will be large and $J_{ph}(0)$ will be significantly less than J_{ph}'' which will result into reduced J_{sc}. Also if R_s is very large, J_{sc} would become small. Therefore to obtain maximum J_{sc}, the internal recombination and difficulty in charge extraction should be minimized. Both of these conditions can be obtained by using the materials of high charge carrier mobilities with optimum nanoscale morphology. Padinger *et al.* [5] studied the photovoltaic response of P3HT : PCBM solar cells, which were subjected to different post-production treatments. The solar cell without any post-production treatment exhibited $V_{oc} = 0.3$ V, $J_{sc} = 2.5$ mA/cm^2, $FF = 0.4$ and power conversion efficiency of 0.4%. When the cell was subjected to heat treatment at 75 °C for 4 min, V_{oc} increased to 0.5 V, J_{sc} increased to 7.5 mA/cm^2, FF increased to 0.57 and power conversion efficiency increased to 2.5%. Apart from that, a solar cell subjected to post-production annealing at 75 °C with simultaneous application of an external voltage greater than V_{oc} gives $V_{oc} = 0.55$ V, $J_{sc} = 8.5$ mA/cm^2, $FF = 0.6$ and power conversion efficiency of 3.5%. Post-production treatment resulted into great increment in rectification ratio because of burning of shunt and improved nanoscale morphology. Burning of shunts and improved morphology reduce recombination losses, which correspond to increment in R_{p2}. Post-production annealing enhances the crystallization of the polymer, which imparts better charge carrier mobility in the active layer. The improved charge carrier mobility reduces R_s in PSCs. The crystallization effect is added with orientational effect of polymer chains due to external applied voltage that improves further the mobility of charge carriers. Therefore, increment in R_{p2} and reduction in R_s result into improved J_{sc}, which is quite in agreement with Equation (13). Howard *et al.* have shown that nanoscale morphology has a crucial effect on charge carrier generation and recombination in P3HT : PCBM system [42]. Li *et al.* have shown that controlling the morphology of active layer, one can increase the charge carrier mobility in P3HT : PCBM systems, which reduces R_s, resulting into increased J_{sc} [24]. However even when J_{sc} is not equal to J_{ph}'', we can obtain J_{ph}'' at application of some reverse bias because in that case the voltage across D3 will decrease and eventually when D3 is *off*, the recombination through D3 will become zero and we obtain maximum extractable photocurrent J_{ph}''. This is quite consistent with the results observed in Figure 6. If the current near short circuit condition shows good saturation, J_{sc} will be equal to J_{ph}''. If current does not show saturation at short circuit condition, it represents great recombination losses, which should be minimized to realize high efficiencies.

For $0 < V < V_{bi}$, the voltage drop across D4 would decrease, which will result into reduction in output photocurrent contribution (J_{ph}') and increment in recombination losses. However, the nonlinear reduction in J_{ph}' in this region (Figure 5) can be understood in terms of recombination of charge carriers through D3, R_{p2}, D1 and R_p and exponential variation of J_{ph} through D4. At a particular + ve voltage, the voltage drop across D4 would become zero and there will be no extraction of photocurrent; all the photo-generated charge carriers will recombine through D3 and R_{p2}. In this situation $J_{ph}(V)$ would become 0 resulting into $J_{ph}' = 0$. This is the situation which will happen at $V = V_{bi}$, which is 0.66 V in the present case (Figure 5). The voltage at which photocurrent becomes 0 corresponds the point of intersection of dark and illuminated *J–V* characteristics and has been observed by several other groups as well [30,36].

In open circuit condition, J_{ph}' will be equal and opposite to the current due to applied voltage, which will result into net zero current through R_s. J_{ph}' will now be equal to J_{ph} (V_{oc}). Therefore, V_{oc} of the cell can be determined from the condition:

$$J_{s1}(V_{oc})\left(\exp\left(\frac{qV_{oc}}{n_1kT}\right) - 1\right) + \frac{V_{oc}}{AR_p} - J_{ph}(V_{oc}) = 0. \quad (14)$$

where $J_{ph}(V_{oc}) = J_{ph}'' - J_{RR2}(V_{oc})$ and $J_{RR2}(V_{oc})$ is the recombination current through R_{p2}. For open circuit condition, D2 will be *off* and the current through it will be negligible. It can be inferenced clearly from Equation (14) that at a given illumination intensity, the V_{oc} will be maximum, if recombination is minimum, or in other words V_{oc} can be improved by minimizing the recombination losses. For no recombination losses, the photocurrent would be maximum and we will obtain maximum V_{oc}. The recombination losses can be minimized by increasing R_p and R_{p2} via improving the nanoscale morphology. This observation is well supported by the results observed by Padinger *et al.*, where post-production treatment burns the shorts and increases shunt resistance and increment in shunt resistance enhances V_{oc} from 0.3 to 0.55 V [5]. It can be seen clearly from Figure 7 or from Equation (14), that R_s does not have any effect on V_{oc}. This fact is well supported by the experimental data from different groups [24,43].

For $V > V_{bi}$, D4 will be reverse biased and no photocurrent would be extracted out through this circuit and it becomes passive. Now in that case, the second circuit component (encircled portion A, Figure 7), would become active as the zener diode D7 is now short circuited. Now the direction of flow of photocurrent will become reversed and will add to the dark current. In this case, the current source comprises a reservoir of charge carriers but not the voltage source. The charge carriers are extracted by the applied electric field. The maximum current through this

reservoir can be some multiple of J_{ph}''. Although for $V > V_{bi}$ the direction of photocurrent is changed but recombination and collection will happen in this case as well. Similar to the previous case, this situation can also be described by introduction of two more diodes such that one diode (D5) is for recombination losses and the other (D6) is for charge extraction. D5 and D6 are connected in such a way that they have importance under illumination only. In dark they are reverse biased and do not contribute. The current through D5 along with R_{p3} corresponds to recombination losses and the current through D6 along with R_{s3} corresponds to extracted current $J_{ph}(V)$. In principle, R_{s3} and R_{p3} are equal to R_{s2} and R_{p2}, respectively. Because of exponential variation of photocurrent with applied voltage, the use of diodes is justified. For $V > V_{bi}$, D5 will be in reverse bias and photo-generated charge carriers will be extracted through D6. The extracted photocurrent increases exponentially with applied voltage until it saturates to some multiple of J_{ph}''. The change in series resistance under illumination can be explained by variation of photo-induced R_{p3} and R_{s3}. Variation in photo-induced series and shunt resistances cannot be ignored with variation in temperature, as it is a crucial parameter for determination of J_{sc}, V_{oc} and *FF* [44,45]. J_{sc} and *FF* reduce whereas V_{oc} increases with reduction in temperature [45]. According to Equations (13) and (14), the reductions in J_{sc} and V_{oc} can be attributed to increment in series resistance and reduction in shunt resistance, respectively. This fact is well supported by the experimental data by Riedel *et al*. where series resistance increases and shunt resistance decreases with reduction in temperature [45].

On the basis of the aforementioned model, we could explain various other important features observed for PSCs. Reduction in J_{ph}' at very high reverse bias (Figure 6) is because of the reason that photocurrent through D4 has saturated and the current due to applied voltage through D2 increases rapidly, therefore, the difference between illuminated and dark current (J_{ph}') decreases. In case of forward bias when photocurrent has saturated through D6, the current through D1, due to applied voltage, increases very rapidly and the difference between light and dark current (J_{ph}') decreases. We did measure the characteristics even with larger voltage range (± 5 V) but could not explain the observed results. It can be attributed to the change in device physics at very high voltages, as current may become space charge limited and the aforementioned model will not be applicable. J_{ph}' increases with increment in illumination intensity and can be attributed to increment in J_{ph}'' due to increased exciton generation rate. Figure 8 shows the measured J_{sc}, V_{oc} and *FF* at different illumination intensities. J_{sc} increases linearly, *FF* decreases almost linearly, whereas V_{oc} increases first rapidly and then saturates with increment in illumination intensity. Increment in J_{sc} with increment in illumination intensity can be attributed to increment in $J_{ph}(0)$ due to increment in J_{ph}'' as the exciton generation rate increases. Calculations show that the current under illumination exhibits poor saturation near short circuit

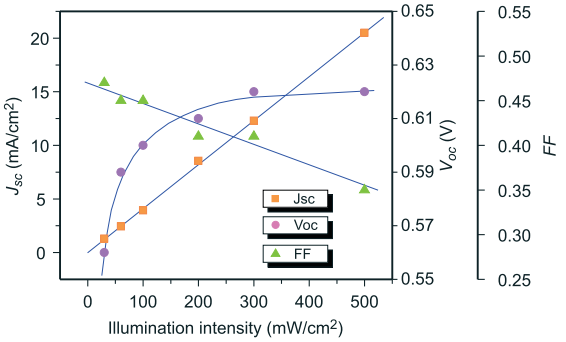

Figure 8. Variation in J_{sc}, V_{oc} and *FF* with illumination intensity for the studied ITO/PEDOT : PSS/P3HT : PCBM/Al solar cell. Symbols represent experimental data and solid curves have just been plotted to guide the eyes about the trend in variation.

condition for low charge carrier mobilities, however, saturation could be observed at large reverse bias. High charge carrier mobilities would result in saturation very near to the short circuit condition. Increment in V_{oc} with illumination intensity can be attributed to increment in $J_{ph}(V_{oc})$, resulting to large voltage drop across R_p in open circuit condition (Equation (14)). For very large illumination intensity, V_{oc} would saturate but will remain less than V_{bi} as some voltage would drop across R_{s2} as well. It can be seen clearly from the equivalent circuit model that if somehow V_{bi} increases, it will result into increment in V_{oc} and its saturation value. Please note that V_{bi} is controlled by the difference of work functions of anode and cathode materials. Variation in either electrode would result variation in V_{oc}, provided Fermi levels of the electrodes are not pinned at the energy levels of organic materials. These results are well supported by the experimental data, where V_{oc} increases because of increment in V_{bi} [46,47]. Similarly reduction in *FF* with illumination intensity can be attributed to reduction in shunt resistance and increment in series resistance. It is also observed that J_{sc} and V_{oc} change with temperature, where J_{sc} decreases and V_{oc} increases with reduction in temperature [48]. Reduction in J_{sc} with temperature can be attributed to reduction in R_{p2} due to reduction in charge carrier mobilities. Reduction in R_{p2} would result into large recombination losses resulting reduction in $J_{ph}(0)$ and J_{sc}, whereas increment in V_{oc} can be attributed to increment in V_{bi} at low temperatures [36]. It is seen from the aforementioned model that J_{ph}'' can be obtained in reverse bias with large applied voltages. Once J_{ph}'' is known, R_{p2} can be calculated from the condition when J_{ph}' becomes 0 at $V = V_{bi}$, as in that case the current through R_{p2} would be J_{ph}'' and R_{p2} can be obtained from $(V_{bi} - JAR_s)/J_{ph}''$, where J is the output current at $V = V_{bi}$. Once R_{p2} is known, R_{s2} can also be determined from the Kirchhoff's law. Optimization of R_{s2} and R_{p2} would minimize the internal losses and would lead to efficient devices. Depending upon the device properties, the extrinsic series and shunt resistances would also have significant impact on the performance even with optimized internal resistances.

5. CONCLUSION

We have analyzed in detail the dark and illuminated characteristics of P3HT : PCBM solar cells and examined the applicability of conventional circuit model. The conventional circuit model was found inadequate for PSCs and an improved model was required to explain the characteristics. First we developed a model for *J–V* characteristics in dark and under illumination, and then based on that an equivalent circuit model was developed. The model explains correctly the nature of characteristics with different illumination intensities and different temperatures as well. The central assumption under illumination is that the photocurrent is not constant but varies with applied voltage and the direction of flow of photocurrent changes with change in the direction of internal electric field, which is given by $(V_{bi} - V)d$. The model is developed by treating reverse and forward bias separately for both the dark and illuminated conditions. The equivalent circuit in light for $V < V_{bi}$ is proposed to be different from that for $V > V_{bi}$. The model enabled us to understand that for no recombination both the photocurrent and photovoltage would be maximum and would result into maximum power conversion efficiency. Therefore for high efficiencies, the recombination losses should be minimized and it can be realized via using materials with excellent electronic properties and excellent interface formation.

ACKNOWLEDGEMENTS

Authors would like to thank Prof. R. C. Budhani, Director NPL, New Delhi, for his keen interest and support to the work. One of us (AG) is thankful to the Department of Science and Technology for awarding the Inspire Fellowship. Financial support from CSIR-India is also acknowledged.

REFERENCES

1. Kumar P, Chand S. Recent progress and future aspects of organic solar cells. *Progress in Photovoltaics: Research and Applications* 2011; **20**: 377.
2. Dennler G, Scharber MC, Brabec CJ. Polymer-fullerene bulk-heterojunction solar cells. *Advanced Materials* 2009; **21**: 1323.
3. Helgesen M, Sondergaard R, Krebs FC. Advanced materials and processes for polymer solar cell devices. *Journal of Materials Chemistry* 2010; **20**: 36.
4. Liang Y, Xu Z, Xia J, Tsai ST, Wu Y, Li G, Ray C, Yu L. For the bright future bulk heterojunction polymer solar cells with power conversion efficiency of 7.4 %. *Adv. Mater.* 2010; **22**: E135.
5. Padinger F, Rittberger RS, Sariciftci NS. Effects of post production treatment on plastic solar cells. *Advanced Functional Materials* 2003; **13**: 85.
6. Ma W, Yang C, Gong X, Lee K, Heeger AJ. Thermally stable, efficient polymer solar cells with nanoscale control of the interpenetrating network morphology. *Advanced Functional Materials* 2005; **15**: 1617.
7. Liang Y, Feng D, Wu Y, Sai ST, Li G, Ray C, Yu L. Highly efficient solar cell polymers developed via fine-tuning of structural and electronic properties. *Journal of the American Chemical Society* 2009; **131**: 7792.
8. Kim JY, Lee K, Coates NE, Moses D, Nguyen TQ, Dante M, Heeger AJ. Efficient tandem polymer solar cells fabricated by all-solution processing. *Science* 2007; **317**: 222.
9. Shaheen SE, Brabec CJ, Sariciftci NS, Padinger F, Fromherz T, Hummelen JC. 2.5 % efficient organic plastic solar cells. *Applied Physics Letters* 2001; **78**: 841.
10. www.solermer.com.
11. Green MA, Emery K, Hishikawa Y, Warta W. Solar cell efficiency tables. *Progress in Photovoltaics: Research and Applications* 2010; **18**: 144.
12. http://pv-tech.org/news/_c/opv_dssc.
13. Hauch JA, Schilinsky P, Choulis SA, Childers R, Biele M, Brabec CJ. Flexible organic P3HT:PCBM bulk-heterojunction modules with more than 1 year outdoor lifetime. *Solar Energy Materials and Solar Cells* 2008; **92**: 727.
14. Krebs FC. Encapsulation of polymer photovoltaic prototypes. *Solar Energy Materials and Solar Cells* 2006; **90**: 3633.
15. Lungenschmied C, Dennler G, Neugebauer H, Sariciftci NS, Glatthaar M, Meyer T, Meyer A. Flexible, long-lived, large area, organic solar cells. *Solar Energy Materials and Solar Cells* 2007; **91**: 379.
16. Meng X, Zhang W, Tan Z, Li Y, Ma Y, Wang T, Jiang L, Shu C, Wang C. Highly efficient and thermally stable polymer solar cells with dihydronaphthyl-based [70] fullerene bisadduct derivative as the acceptor. *Advanced Functional Materials* 2012 (in press).
17. Sun Y, Takacs CJ, Cowan SR, Seo JH, Gong X, Roy A, Heeger AJ. Efficient, air-stable, bulk-heterojunction polymer solar cells using MoOx as the anode interfacial layer. *Advanced Materials* 2011; **23**: 2226.
18. Yun JM., Yeo JS, Kim J, Jeong HG, Kim DT, Noh YJ, Kim SS, Ku BC, Na SI. Solution processable reduced graphene oxide as a novel alternative to PEDOT:PSS hole transport layers for highly efficient and stable polymer solar cells. *Advanced Materials* 2011; **23**: 4923.
19. Nalwa KS, Carr JA, Mahadevapuram RC, Kodali HK, Bose S, Chen Y, Petrich JW, Ganapathysubramanian B, Chaudhary S. Enhanced charge separation in organic photovoltaic films doped with ferroelectric diopoles. *Energy & Environmental Science* 2012; **5**: 7042.
20. Shoaee S, Clarke TM, Huang C, Barlow S, Marder SR, Heeney M, McCulloch I, Durrant JR. Acceptor energy level control of charge photogeneration in organic donor/acceptor blends. *Journal of the American Chemical Society* 2010; **132**: 12919.

21. Yuan Y, Reece TJ, Sharma P, Poddar S, Ducharme S, Gruverman A, Yang Y, Huang J. Efficiency enhancement in organic solar cells with ferroelectric polymers. *Nature Materials* 2011; **10**: 296.
22. Peet J, Kim JY, Coates NE, Ma WL, Moses D, Heeger AJ, Bazan GC. Efficiency enhancement in low-bandgap polymer solar cells by processing with alkane dithiols. *Nature Materials* 2007; **16**: 497.
23. van Duren JKJ, Yang X, Loos J, Bulle-Lieuwma CWT, Sieval AB, Hummelen JC, Janssen RAH. Relating the morphology of poly(phenylene vinylene)/methanofullerene blends to solar cell performance. *Advanced Functional Materials* 2004; **14**: 425.
24. Li G, Shrotriya V, Huang J, Yao Y, Moriarty T, Emery K, Yang Y. High efficiency solution processable polymer photovoltaic cells by self-organization of polymer blends. *Nature Materials* 2005; **4**: 864.
25. Jain A, Kapoor A. A new approach to study organic solar cell using Lambert W-function. *Solar Energy Materials and Solar Cells* 2005; **86**: 197.
26. Potscavage WJ, Jr., Sharma A, Kippelen B. Critical interfaces in organic solar cells and their influence on the open circuit voltage. *Accounts of Chemical Research* 2009; **42**: 1758.
27. Araujo GL, Sanchez E, Marti M, Determination of the two exponential solar cell equation parameters from empirical data. *Solar Cells* 1982 ; **5**: 199.
28. Mazhari B. An improved solar cell circuit model for organic solar cells. *Solar Energy Materials and Solar Cells* 2006; **90**: 1021.
29. Sze SM. *Physics of Semiconductor Devices*. Wiley: New York, 1981.
30. Schilinsky P, Waldauf C, Hauch J, Brabec CJ. Simulation of light intensity dependent current characteristics of polymer solar cells. *Journal of Applied Physics* 2004; **95**: 2816.
31. Jain SC, Willander M, Kumar V. *Conducting Organic Materials and Devices*. Academic Press: San Diego, 2007.
32. Kumar P, Jain SC, Kumar V, Chand S, Tandon RP. A model for J-V characteristics of P3HT:PCBM solar cells. *Journal of Applied Physics* 2009; **105**: 104507.
33. Belmonte GG, Munar A, Barea EM, Bisquert J, Ugarte I, Pacios R. Charge carrier mobility and lifetime of organic bulk heterojunctions analyzed by impedance spectroscopy. *Organic Electronics* 2008; **9**: 847.
34. Kumar P, Kumar H, Jain SC, Venkatesu P, Chand S, Kumar V. Effect of active layer thickness on open circuit voltage in organic photovoltaic devices. *Japanese Journal of Applied Physics* 2009; **48**: 121501.
35. Cracium NI, Brondijk JJ, Blom PWM. Diffusion enhanced hole transport in thin polymer light emitting diodes. *Physical Review B* 2008; **77**: 35206.
36. Kumar P, Jain SC, Kumar H, Chand S, Kumar V. Effect of illumination intensity and temperature on open circuit voltage in organic solar cells. *Applied Physics Letters* 2009; **94**: 183505.
37. Hoppe H, Arnold N, Sariciftci NS, Meissner D. Modeling the optical absorption within conjugated polymer/fullerene based bulk-heterojunction organic solar cells. *Solar Energy Materials and Solar Cells* 2003; **80**: 105.
38. Koster LJA, Smits ECP, Mihailetchi VD, Blom PWM. Device model for the operation of polymer/fullerene bulk heterojunction solar cells. *Physical Review B* 2005; **72**: 85205.
39. Lee MK, Wang JC, Horng SF, Meng HF. Extraction of solar cell series resistance without presumed current-voltage function form. *Solar Energy Materials and Solar Cells* 2010: **94**: 578.
40. Ramsdale CM, Barker JA, Arias AC, MacKenzie JD, Friend RH, Greenham NC. The origin of the open circuit voltage in polyfluorene-based photovoltaic devices. *Journal of Applied Physics* 2002; **92**: 4266.
41. Waldauf C, Schilinsky P, Hauch J, Brabec CJ. Materials and device concepts for organic photovoltaics: towards competitive efficiencies. *Thin Solid Films* 2004; **451-452**: 503.
42. Howard IA, Mauer R, Meister M, Laquai F. Effect of morphology on ultrafast free carrier generation in polythiophene:fullerene organic solar cells. *Journal of the American Chemical Society* 2010; **132**: 14866.
43. Servaites JD, Yeganeh S, Marks TJ, Ratner MA. Efficiency enhancement in organic photovoltaic cells: consequences of optimizing series resistance. *Advanced Functional Materials* 2010; **20**: 97.
44. Thakur AK, Wantz G, Belmonte GG, Bisquert J, Hirsch L. Temperature dependence of open circuit voltage and recombination processes in polymer-fullerene based solar cells. *Solar Energy Materials and Solar Cells* 2011; **95**: 2131.
45. Riedel I, Parisi J, Dyakonov V, Lutsen L, Vanderzande D, Hummelen JC. Effect of temperature and illumination on the electrical characteristics of polymer-fullerene bilk-heterojunction solar cells. *Advanced Functional Materials* 2004; **14**: 38.
46. Mihailetchi VD, Blom PWM, Hummelen JC, Rispens MT. Cathode dependence of the open circuit voltage of polymer:fullerene bulk heterojunction solar cells. *Journal of Applied Physics* 2003; **94**: 6849.
47. Uhrich C, Wynands D, Olthof S, Riede MK, Leo K, Sonntag S, Maennig B, Pfeiffer M. Origin of open circuit voltage in planer and bulk heterojunction organic thin-film photovoltaics depending on doped transport layer. *Journal of Applied Physics* 2008; **104**: 43107.
48. Katz EA, Faiman D, Tuladhar SM, Kroon JM, Wienk MM, Fromherz T, Padinger F, Brabec CJ, Sariciftci NS. Temperature dependence for the photovoltaic device parameters of polymer-fullerene solar cells under operating conditions. *Journal of Applied Physics* 2001; **90**: 5343.